



Gazi University

Journal of Science

PART A: ENGINEERING AND INNOVATION

<http://dergipark.org.tr/guj.1362103>

Boron-Doped Thin Films Fabricated by the Spin Coating Method: The Effect of Doping Concentrations

Abdullah ATILGAN^{1,2*} Kenan OZEL³ ¹ Department of Energy Systems Engineering, Faculty of Engineering and Natural Sciences, Ankara Yıldırım Beyazıt University, Ankara, Türkiye² Central Research Laboratory Application and Research Center, Ankara Yıldırım Beyazıt University, Ankara, Türkiye³ Department of Electrical and Energy, GAMA Vocational School, Ankara University, Ankara, Türkiye

Keywords	Abstract
Boron Doped ZnO B Doping Spin Coating Method Thin Film	This work examined the impact of different levels of B-doping on the structural, morphological, optical, and electrical characteristics of ZnO thin films. Boron-doped zinc oxide thin films were deposited on glass substrates using the spin-coating technique. The B concentrations employed were 1, 2, 3, 4, and 5 at. %. The systematic characterizations manifest that the properties of the deposited films were heavily influenced by changing concentrations of B doping. It was found that as the concentration of B-doping increases, the values of grain size decrease. In addition, it was observed that ZnO thin films containing a lower concentration of B dopant exhibited higher transparency. Finally, it was figured out that the resistivity of the films declines dramatically with a higher content of B-doping. The results of our research may initiate further inquiries into the creation of superior thin films.
Cite	
Atilgan, A., & Ozel, K. (2024). Boron-Doped Thin Films Fabricated by The Spin Coating Method: The Effect of Doping Concentrations. <i>GU J Sci, Part A, 11(1)</i> , 57-67. doi:10.54287/guj.1362103	
Author ID (ORCID Number)	Article Process
0000-0002-5624-3664	Abdullah ATILGAN
0000-0002-0250-3731	Kenan OZEL
	Submission Date 18.09.2023 Revision Date 19.10.2023 Accepted Date 12.12.2023 Published Date 05.02.2024

1. INTRODUCTION

Zinc oxide (ZO) thin films (TFs) have garnered significant attention in recent decades due to their ability to high infrared reflectance, high visible transmittance, a lower price, and a non-toxic nature (Hu & Gordon, 1992). ZO is classified as an n-type semiconductor due to its electronic properties. It owns a band gap (E_g) of around 3.2 eV. ZO-TFs in their pure form exhibit a notable degree of visible light transmittance and possess a high level of resistance. Non-stoichiometric ZO-TFs show the desirable characteristics of high transparency and high conductivity. However, their stability is compromised when exposed to high temperatures. In contrast, doped ZO-TFs exhibit exceptional stability in terms of their electrical and optical characteristics. ZO-TFs that have been doped with different IIIA elements, like indium, aluminum, gallium, and boron (B), have low electrical resistance and let a lot of light through (Hu & Gordon, 1992; Kara et al., 2017; Kayani et al., 2020, Atilgan et al., 2023).

Previous study has indicated that the E_g of ZO-TFs, even with high B concentrations of up to 1.4 at. %, did not undergo major changes (Tahar & Tahar, 2005). The observed impact on the optical E_g property and conductivities of TFs was significant, even at a minimal B concentration of 0.2 at.%. The reported range of conductivities spanned from 250 to 2500 $\Omega^{-1} \text{ cm}^{-1}$ (Hu & Gordon, 1992). Lokhande et al. (2001) utilized the spray pyrolysis method to coat TFs with B dopant ranging from 0 to 1 at.%. They observed a decrease in resistance and an increase in E_g . The researchers documented that the ideal doping concentration for achieving good optical transmittance and low resistance was determined to be 0.8 at.%. In contrast, the introduction of B doping has been seen to enhance the density and mobility of carriers within ZO-TFs, as a result of which

their electrical conductivity has increased. The introduction of B doping into ZO results in an enhancement of its magnetic moment, a characteristic that distinguishes it from the magnetic properties observed in ZO doped with other elements. Nevertheless, the existing body of literature reveals a limited number of studies pertaining to the synthesis of B-doped zinc oxide (B-ZO) TFs. These TFs have predominantly been created using various methods such as electrochemical deposition, atomic layer deposition, chemical vapor deposition, spray pyrolysis, and RF magnetron sputtering (Hu & Gordon, 1992). Conversely, their systems exhibit a high degree of complexity, substantial cost implications, and pose challenges in terms of manageability. Hence, owing to its user-friendly nature and enhanced film quality, sol-gel synthesis, namely sol-gel, spin-coating, and dip-coating, has emerged as a prominent method for the fabrication of B-ZO-TFs. The primary benefits of sol-gel synthesis encompass its simplicity and cost-effectiveness, its facilitation of ZO doping with diverse elements, its independence from complex equipment or hazardous source materials, and its efficacy in efficiently coating ZO-TFs (Lee et al., 2013). The sol-gel technique has numerous benefits, including enhanced homogeneity, purity, cost-effectiveness, the ability to be deposited on vast substrate surfaces, precise compositional control, and simplicity of handling (Kayani et al., 2020). Ozel and Atilgan were investigated the synergistic effect of gallium and boron co-doping on the optical and electrical features of ZO-TFs using spin coating technique. The sample with a B/Ga ratio of 0.5/2.5, while keeping a constant total doping rate of 3 at. %, exhibited superior properties compared to the sample with a B/Ga ratio of 0/3. This improvement can be attributed to the synergistic effect of enhanced conductivity and transparency. (Ozel & Atilgan, 2023a).

As for the comparison of widely utilized deposition techniques, spin-coating and spray-pyrolysis offer cost-effective and uncomplicated alternatives to more expensive equipment and high-energy processes associated with other approaches (Zhussupbekova et al. 2020). Utilizing the spray pyrolysis process in a single container with continuous output is its significant advantage. As spray pyrolysis is performed in the micrometer volume and seconds of all the operations described, deviations are possible in the planned experiments, and nanoparticles synthesized based on this method are often metastable (Majerič & Rudolf, 2020). Nevertheless, the spin-coating technique provides excellent consistency in both macroscopic and nanoscale, and it also frequently eliminates the need for subsequent thermal processing. The spin-coating method possesses qualities that render it very suitable for both research purposes and rapid prototype creation. In addition, it is noteworthy to say that spin coating is the mostly preferred method for depositing the ZO-TF on the various substrates thanks to its simplicity, capacity to produce uniform coating, and ease of setup (Farrag & Balboul, 2017; Kamaruddin et al., 2011; Smirnov et al. 2010). Moreover, the spin coating technique not only provides fast and high-quality film production, but also allows the reproducible preparation of TF coatings over large areas with excellent structural homogeneity (Faisal et al., 2015).

The present study investigates the deposition of B-ZO-TFs by utilizing the spin-coating approach. The study focuses on analyzing the electrical, optical, and structural characteristics of the TFs and subsequently presents a comprehensive discussion of the obtained results. Systematically, the impact of B doping concentration on the characteristics of ZO-TFs has been examined. The findings of the characterization indicate that various concentrations of B doping have a substantial effect on the characteristics of the deposited TFs.

2. MATERIAL AND METHOD

B-ZO-TFs with a range of dopant concentrations were spin-coated onto glass substrates (GSs) using a sol-gel process. The transparent solution, made by employing ZADH (zinc acetate dihydrate, $\text{ZnC}_4\text{H}_6\text{O}_4 \cdot 2\text{H}_2\text{O}$; Emsur) as a precursor, trimethyl borate ($\text{C}_3\text{H}_9\text{BO}_3$; Merck) as a dopant, and MAE (monoethanolamine, $\text{C}_2\text{H}_7\text{NO}$; Emsur) as a stabilizer, was dissolved in ethanol (CH_3OH ; Merck). The concentration of ZADH in the ethanol solvent was 0.5 M, and the molar ratio of MEA to ZADH was consistently maintained at a 1:1 molar ratio. The concentration of B dopant ($[\text{n}_\text{B}/[\text{n}_\text{B}+\text{n}_\text{Zn}]])$ was determined to be 1%, 2%, 3%, 4%, and 5 atomic percent, respectively. The resultant solution was agitated at a speed of 500 revolutions per minute (rpm) at a temperature of 25 °C for a duration of 2 hours, resulting in the formation of transparent and uniform solutions. The solutions were allowed to mature for 48 hours at room temperature (RT) prior to being utilized as coating solutions. As for the deposition procedure, the prepared solutions were placed on the surface of GSs, and then the substrates were brought up to a spinning speed of 2000 rpm with an acceleration time of 5 s for a spinning duration of 30 s. The coated GSs were preheated at 500 °C for 5 minutes to remove organic compounds. Ten

cycles of this coating and preheating procedure were performed. Finally, the obtained TFs were annealed at 500 °C for 1 hour to get the polycrystalline oxide TFs.

An X-ray diffractometer (XRD; Rigaku Miniflex 600) was performed to investigate the crystal structure of the deposited TFs. Atomic force microscope (AFM; Ambios-Quesant) measurements were used to analyze the surface morphology and roughness. A UV-vis spectrophotometer (Shimadzu 1700) was utilized to characterize the optical transmittance and absorbance properties of the samples. The electrical sheet resistance values of the TFs were found at RT using the four-point probe method and a Keithley 2400 source meter along with a Lucas Labs 302.

3. RESULTS AND DISCUSSION

Figure 1 (a) illustrates the XRD spectra of ZO-TFs with various B concentrations. The observed diffraction peaks are consistent with the specifications for ZO crystal (JCPDS Card No. 36-1451) (Kayani et al., 2020). The spectra indicate that the TFs exhibit a polycrystalline structure, and no impurity peak is detected. In order to investigate the variation of the grain size with varying doping concentrations, the size of the grains along the (002) plane is determined by using the Debye-Scherrer equation (1) (Kayani et al., 2020);

$$D = \frac{K\lambda}{\beta \cos\theta} \quad (1)$$

where β , λ , and θ stand for the full width of half-maximum (FWHM), the wavelength of X-rays (0.15406 nm), and the Bragg angle, respectively. As the concentration of B doping increases, both the intensity and the FWHM of the (002) peaks exhibit simultaneous changes. Specifically, the intensity of the peaks drops as the FWHM expands. The findings indicate a noticeable drop in both the degree of crystallinity and the diameters of crystalline as the concentration of B doping increases. (Figure 1(b-f) and Table 1). The average crystallite size decreased from 18.8 nm to 14.1 nm due to the increase in B concentration. The decrease seen can be ascribed to the distortion of the ZO lattice subsequent to the injection of B dopants into the ZO material. The observed distortion can be related to the mismatch in ionic radii between B^{3+} (0.23 Å) and Zn^{2+} (0.74 Å). Since the very small ionic radius of additive B in comparison to the Zn ion, it can easily settle in the crystal lattice (Hu & Gordon, 1992). Incorporating B doping into ZO-TFs caused both lattice deformation and the formation of lattice defects and nucleation sites, hence impeding the growth of grains. Heavy doping of B resulted in a reduction in the level of crystallinity and disruption of the crystal symmetry. The findings presented herein exhibit a high level of concordance with the previously reported results. (Jana et al., 2011; Kim et al., 2013).

While the concentration of B in the TFs increases, lattice constants change, and the position of the (002) peaks shift towards the higher angles of the 2θ scale. This suggests that the B-ZO-TFs have higher levels of residual stress than strain-free ZO. Besides, the amount of residual stress in the B-ZO-TFs appears to increase with higher concentrations of B in the TFs. There are therefore interstitial Zn^{2+} ions present along with the B^{3+} ions, which move the (002) peak to a greater angle. This phenomenon can be attributed to the reduction in the distance between adjacent crystal planes. Sun et al. (2020) and Kim et al. (2013) tested lower B concentrations of 0-0.5 at.% and 0-2.5 at.%, respectively. They subsequently argued that the shift in the position of the (002) peaks at a higher angle as the concentration of dopant in the ZO-TFs increases. Contrary to this, in a study that set out to determine dopant concentrations 1, 3, 5, 7, and 9 wt.%, Kayani et al. (2020) found that the presence of a higher concentration of B dopant leads to the position of the (002) peaks shifting towards the lower angles of the 2θ scale. As an overarching finding in this study, which does not contradict the previous reports, the 002 peaks shift to larger angles up to a critical dopant concentration of 3 % and then shift to lower angle values.

Lattice constants are determined using equations (2, 3):

$$a = \frac{\lambda}{\sqrt{3} \sin \theta_{100}} \quad (2)$$

$$c = \frac{\lambda}{\sin \theta_{002}} \quad (3)$$

where a and c are lattice constants (Kayani et al., 2020). Lattice spacing d is found by applying Bragg's law equation (4):

$$d = \frac{n\lambda}{2 \sin \theta} \quad (4)$$

Table 1. Structural properties of B-ZO-TFs

B Content (at. %)	Lattice constants		Lattice spacing, d_{002} (nm)	D (nm)	Strain ε ($\times 10^3$)	Stress σ (GPa)	δ ($\times 10^3$)
	a (nm)	c (nm)					
1	0.3248	0.5208	0.2604	18.8	-2.11	0.49	2.83
2	0.3246	0.5207	0.2603	17.4	-2.39	0.56	3.30
3	0.3242	0.5205	0.2603	16.1	-2.67	0.62	3.88
4	0.3244	0.5208	0.2604	15.6	-2.11	0.49	4.13
5	0.3244	0.5211	0.2606	14.1	-1.54	0.36	5.06

here n is the order of diffraction and is taken as 1. The presence of dislocation density (δ) signifies the existence of imperfections inside the crystal lattice. The presence of defects and distortions inside a crystalline structure result in an increase in dislocation density, which exhibits an inverse relationship (equation 5) with the size of the crystallite:

$$\delta = D^{-2} \quad (5)$$

where δ represents the dislocation density (Kayani et al., 2020). Dislocation density refers to the concentration of dislocations inside a specific volume of crystalline materials, and it is observed to grow proportionally with the rise in the concentration of B. This is due to an improvement in defects. Strain (ε) in the TFs along the c-axis can be determined by applying equation (6):

$$\varepsilon = \left[\frac{c_{film} - c_{bulk}}{c_{bulk}} \right] \quad (6)$$

The unstrained lattice parameter, denoted as c_{bulk} , was figured out for bulk ZO and found to be 0.521939 nm (Kaur et al., 2015). The observed strain in the thin films is a result of the combined influence of thickness and B doping in ZO. The biaxial strain model can be utilized to determine the stress in TFs. The stress present in the film is determined by the utilization of a biaxial strain model (Kaur et al., 2015).

$$\sigma = -232.8 \times \varepsilon \quad (7)$$

Biaxial stress shows tensile characteristics when the stress sign is positive, whereas it demonstrates compressive properties in the opposite case. The residual stress levels in the ZO-TFs, which were doped with B concentrations of 1, 2, 3, 4, and 5%, were measured to be 0.49, 0.56, 0.62, 0.49, and 0.36 GPa, respectively. To better understand the relationship between temperature and stress, Kumar et al. (2012) conducted a series of experiments. The annealing temperatures employed in this study spanned from 350 to 550 °C, while the doping ratio of B maintained at a constant level of 0.6 at. % for all the TFs. It is worth noting that the stress in B-ZO-TFs has a first compressive character, transitioning to a tensile state when subjected to annealing temperatures over 450 °C. The results align with the stress levels seen in our research. The presence of both intrinsic and extrinsic stresses is an inherent characteristic of ZO. Intrinsic stress is typically attributed to the

presence of defects and impurities within a material, while extrinsic stress mostly arises from factors such as lattice mismatch, doping, thermal mismatch, and growth conditions (Kumar et al., 2012).

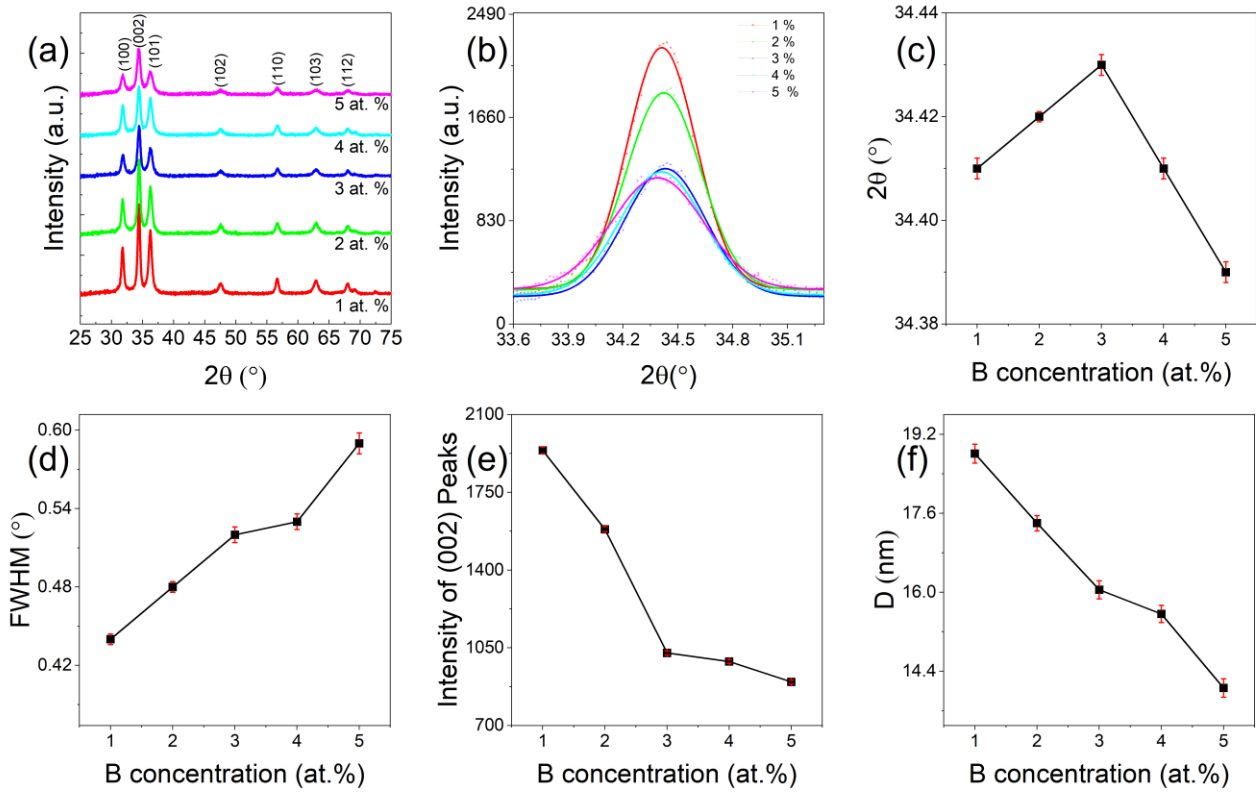


Figure 1. (a) X-ray diffraction patterns for the ZO-TFs with various B contents, (b) 002 diffraction peak fitted with a Lorentz function, (c) position of 002 peaks (2θ), (d) FWHMs, (e) intensity of 002 peaks (f) crystallite sizes of B-ZO-TFs with 1–5% with error bars representing the standard error

Figure 2 (a-f) shows how AFM images are used to look at the surface morphology and roughness of the B-ZO-TFs. The surface parameters, i.e., root mean square RMS, surface area, and volume of B-ZO-TFs, have been calculated using Gwyddion software (Nečas & Klapetek, 2012). The values of skewness and kurtosis for 1, 2, 3, 4, and 5% are 0.47 and 0.24, 0.35 and 0.20, 0.37 and 0.13, 0.49 and 0.27, 0.69 and 0.79, respectively, and point out that the surfaces have more high peaks and fewer valleys and surfaces. As evaluated from AFM results, RMS values are examined to be 80.9, 67.4, 99.7, 72.3, and 33.9 nm for the B-ZO-TFs having a B content of 1%, 2%, 3%, 4%, and 5%, respectively. Values of RMS and volume of TFs showed a similar trend. TF with 1% doping had the highest surface area improvement, and the highest roughness was observed in TF with 3% doping. The complete set of obtained results is presented in Table 2.

The absorbance, absorption coefficient, and transmittance characteristics of B-ZO-TFs are illustrated in Fig. 3 (a–c). As seen in Figure 3 (a), the absorbance profiles of the samples exhibit a sharp absorption edge at around 380 nm, indicating that these TFs might be used in UV photodetector applications (Ozel & Yildiz, 2021). Note that the absorbance profiles of the TFs are substantially affected by the doping process. Specifically, the B-ZO film with a B doping concentration of 3% shows enhanced absorption characteristics through the solar spectrum. Based on this result, one can expect that the photovoltaic cells fabricated with B-ZO TFs with a B content of 3% have better power conversion efficiency than others due to their high absorption ability of incoming light. As for the transmittance spectra of the TFs, the average transmittance values of the TFs are estimated between 400 and 800 nm wavelength and listed in Table 2. Moreover, the transmittance values at 550 nm, which correspond to the maximum intensity value of the solar spectrum at sea level (Ozel et al., 2023), are determined and given in Table 2. The highest transmittance values among the films are obtained 85.3%, 83.6% for 2% and 1%, respectively. The values of the optical E_g for the deposited TFs are evaluated by

calculating the absorption coefficient (α), which is obtained from transmittance data. It can be determined by the equation (8);

$$\alpha = \frac{\ln T^{-1}}{t} \quad (8)$$

where t and T denote the thickness and transmittance of the TFs, respectively (Tahar & Tahar, 2005). In the direct band gap semiconductor, the relationship between α and E_g can be estimated by using the relation (9) (Hu & Gordon, 1992);

$$(\alpha hv)^2 = A(hv - E_g) \quad (9)$$

where hv and A refer to the photon energy and the band edge constant, respectively. Figure 3(d) presents the plots of $(\alpha hv)^2$ versus hv for the obtained B-ZO-TFs. The linear nature of the plots suggests the presence of a direct transition. The E_g values of the TFs can be acquired from extrapolation of the linear portions to $\alpha hv=0$ in the plots $(\alpha hv)^2$ versus hv . Thin-film band-gap values are 3.27 eV, 3.26 eV, 3.23 eV, 3.24 eV, and 3.26 eV, which correspond to 1, 2, 3, 4, and 5%, respectively. From the estimated values, it can be deduced that the E_g values of the B-ZO-TFs are lower than the pristine ZO-TFs (Tan et al., 2005). The obtained values are summarized in Table 2. According to the acquired values of E_g , one can notice that the values of E_g get reduced to some extent with the increase of B content from 1 to 3%. On the other hand, the values of E_g get wider by further B dopants. These slight changes might be related to the formation of localized states and carrier concentration (Kara et al., 2017; Sbeta et al., 2018). Kumar et al. (2012) reported that the E_g of B-ZO-TFs decreased with an increase in annealing temperature and had a strong dependence on the stress of TFs. Our results are in agreement with the E_g and stress values obtained from similar annealing temperatures (Kumar et al., 2012). With increasing stress, E_g narrows, and when stress begins to decrease, E_g begins to expand, although it is still in the positive region. The Swanepoel method was used to determine the thicknesses of the B-ZO-TFs thin film. The approach showed B-ZO-TFs have thicknesses of 881 ± 5.2 nm. The results of Swanepoel, an optical method, were confirmed by Hacini et al. by comparing them with measured values for cross sectional SEM results. The results of both are quite similar, proving the validity of the optical method (Hacini et al., 2021).

Four-point probe I-V curves and the plot of the values of resistivity (ρ) of B-ZO-TFs as a function of B content are depicted in Figure 4(a, b). To calculate the ρ values of the TFs, the sheet resistance (R_{sh}) values are first determined using the following formula (10) (Atilgan et al., 2021);

$$R_{sh} = \frac{\pi}{\ln(2)} \left(\frac{V}{I} \right) \quad (10)$$

where $\pi/\ln 2$ is the geometric correction factor. V and I refer to the values of measured voltage and current, respectively. By calculating R_{sh} , the ρ values of the TFs are determined by $\rho = R_{sh}t$. Note that the obtained values of ρ are consistent with the literature (Senol et al., 2015). According to our findings, one can figure out that the values of ρ decrease to moderate levels with increasing B content. B is a dopant of the n-type that can either replace zinc atoms or occupy interstitial positions within the crystal lattice. This substitution or interstitial incorporation of boron atoms leads to an increase in the density of free electrons inside the TFs. Consequently, this phenomenon leads to an elevation in the concentration of free carriers, resulting in a reduction in resistivity (Lokhande et al., 2021). At doping concentrations from 1 to 3%, the resistance decreased sharply, but at doping concentrations above 3%, the resistance value remained almost constant. There are two possible explanations for this phenomenon. Firstly, at high-levels of doping, the impact of grain boundary scattering is rather insignificant compared to the scattering mechanisms that occur within the grains themselves. Alternatively, this behavior might be attributed to the limitations imposed by the solubility of B dopant elements in the lattice of ZO as a host material (Steinhauser et al., 2007; Kim et al., 2013; Pawar et al., 2005).

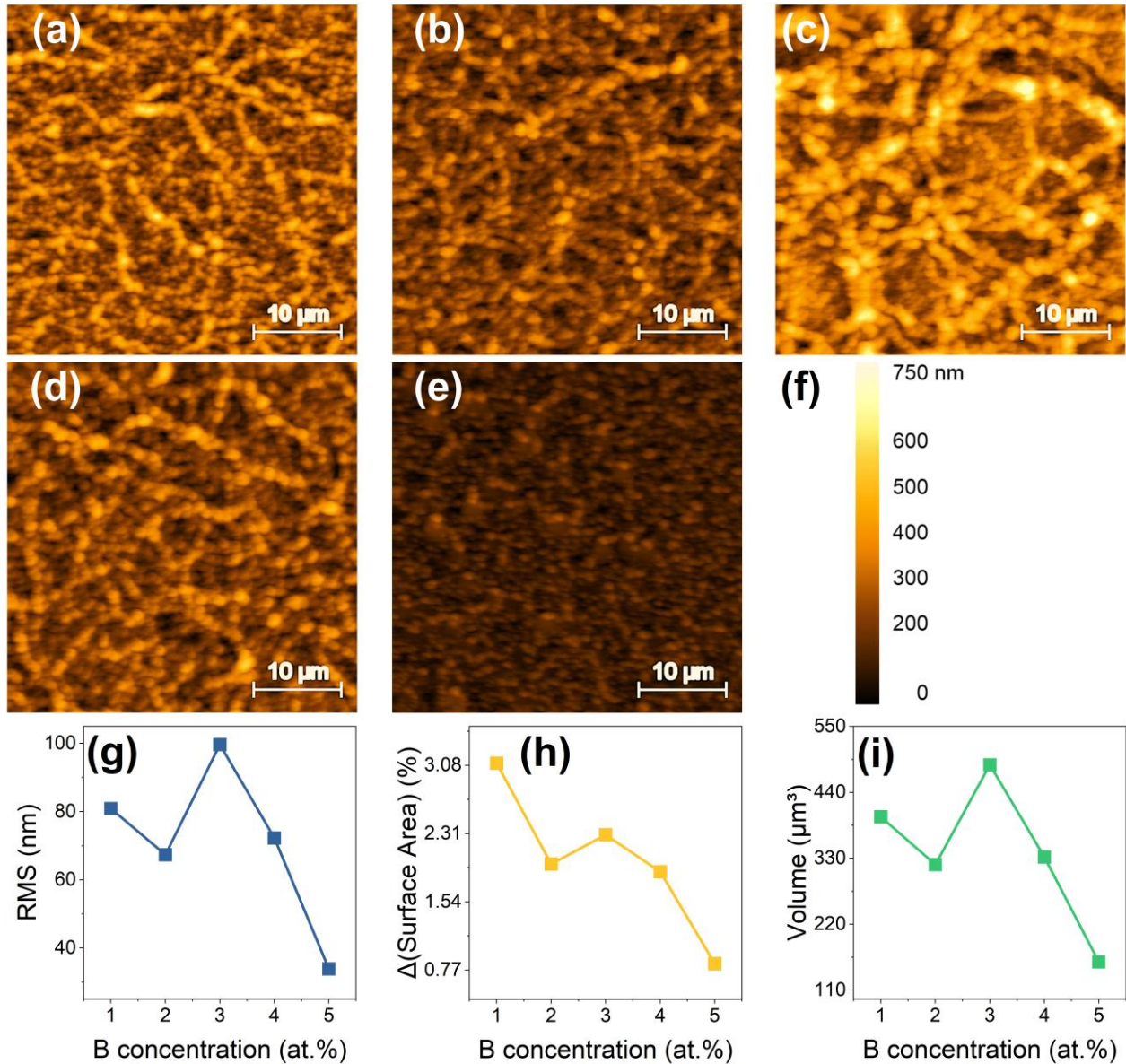


Figure 2. 2D AFM images of the B-ZO-TFs with different various concentration of B (a) 1, (b) 2, (c) 3, (d) 4, (e) 5, (f) The color code shows the scale bar for the height in the image, (g) RMS values, (h) surface areas improvement (i) volume of B-ZO-TFs

Ultimately, our findings reveal that the characteristics of the sol-gel-derived ZO-TFs can be altered by varying the levels of B doping. Based on the acquired findings, it can be posited that optical characteristics exhibit favorable attributes at lower levels of doping, while electrical qualities demonstrate enhanced performance at higher levels of doping.

Table 2. Structural and optical characteristics of the B-ZO-TFs for various B contents

B Content (at. %)	RMS (nm)	T_{av} (%) (400-800nm)	T (%) @550nm	E_g (eV)
1 %	80.9	83.9 ± 7.08	83.6	3.27 ± 0.001
2 %	67.4	83.4 ± 5.69	85.3	3.26 ± 0.001
3 %	99.7	62.0 ± 9.94	61.5	3.23 ± 0.006
4 %	72.3	69.3 ± 8.84	70.4	3.24 ± 0.003
5 %	33.9	72.7 ± 9.69	75.0	3.26 ± 0.002

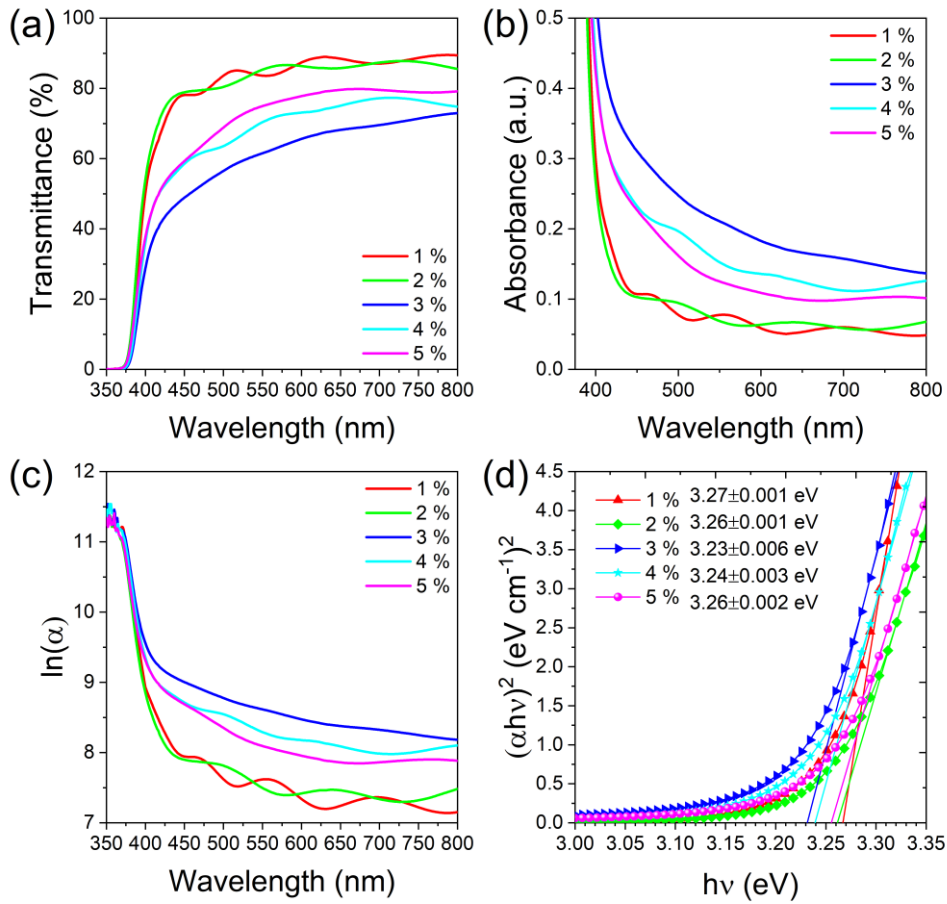


Figure 3. (a) transmittance and (b) absorbance characteristics of B-ZO-TFs fabricated with different doping concentrations. (c) $\ln(\alpha)$ versus wavelength for various B content (d) The plots of $(\alpha h\nu)^2$ versus photon energy ($h\nu$) for TFs doped with 1-5% B content. Band gap values were calculated using linear regression, which aims to find a linear relationship to describe the correlation between a dependent variable. The E_g values are given as the average of the intercept constant \pm standard error of the intercept

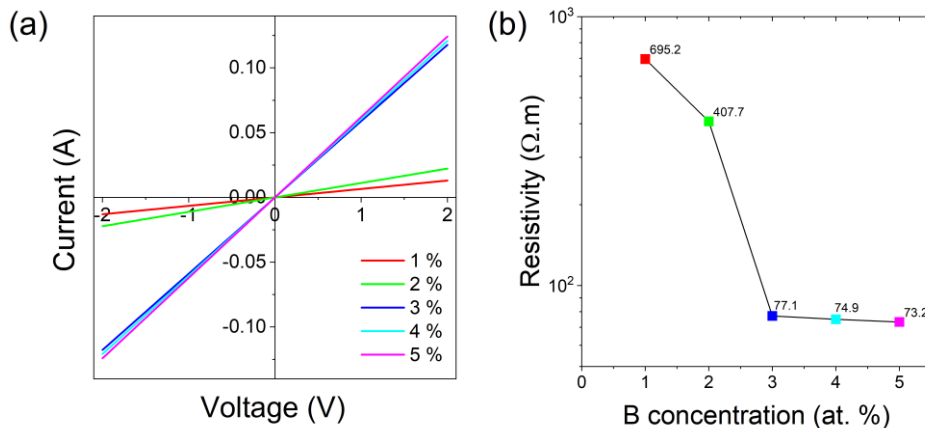


Figure 4. (a) Four-point probe I-V curves showing sheet resistance and (b) plots of the values of resistivity of B-ZO-TFs as a function of B content

4. CONCLUSION

In summary, B-doped ZO-TFs were successfully deposited on GSs by using the spin coating method. We investigated the structural, morphological, optical, and electrical properties of B-doped ZO films, focusing on

the effect of varying the B content. The findings revealed that various B-doping concentrations significantly affected the characteristics of deposited films:

- The values of grain size decrease with an increase in B-doping concentration.
- The surface roughness of the TFs has a trend of fluctuation with the increase in doping concentration of B. While the highest surface roughness was observed in the film with 3% doping, the highest surface area was observed in the film with 1% doping.
- The ZO-TFs containing a lower concentration of B dopant exhibit high transparency above 80%. In addition to this, the best absorption capability was obtained at 3% B-ZO-TFs.
- The 3% B doping rate is the saddle point for E_g , σ , T%, and resistivity values. Up to 3%: While R, E_g , and T tend to decrease, after the saddle point, R remains almost constant and E_g and T tend to increase, respectively. Stress values increase up to the saddle point and then suddenly decrease.

Eventually, it was figured out that the resistivity of the films exhibits a substantial decrease as the B-doping concentration raises. The results of our study have the potential to stimulate further research in the field of thin film development for the purpose of creating advanced optoelectronic devices. The saddle point of doping concentration to gain the best optical and electrical properties is changing depending on the crystalline sizes and stress values of TFs. In other words, the optimal B doping concentration for ZO-TFs may depend on the annealing temperature. Future studies should explore the effects of various annealing temperatures versus doping concentrations with narrow steps.

ACKNOWLEDGEMENT

We are grateful to Prof. Dr. A. YILDIZ and Prof. Dr. M. N. SBETA for their providing the necessary laboratory facilities for the realization of this study.

AUTHOR CONTRIBUTIONS

A.A. and K.O. contributed to the design and implementation of the research, to the analysis of the results and to the writing of the manuscript. All authors have read and legally accepted the final version of the article published in the journal.

CONFLICT OF INTEREST

The authors declare no conflict of interest.

REFERENCES

- Atilgan, A., Ozel, K., Sbeta, M., & Yildiz, A. (2023). Engineering the visible light absorption of one-dimensional photonic crystals based on multilayers of Al-doped ZnO (AZO) thin films. *Materials Science in Semiconductor Processing*, 166, 107747. <https://doi.org/10.1016/j.mssp.2023.107747>
- Atilgan, A., Kurtulus, A. Y., Oktem, M. F., & Yildiz, A. (2021). W-doped ZnO transparent conducting nanostructures synthesized by hydrothermal method. *Journal of Materials Science: Materials in Electronics*, 32(14), 19126-19135. <https://doi.org/10.1007/s10854-021-06432-1>
- Faisal, M., Bouzid, H., Harraz, F. A., Ismail, A. A., Al-Sayari, S. A., & Al-Assiri, M. S. (2015). Mesoporous Ag/ZnO multilayer films prepared by repeated spin-coating for enhancing its photonic efficiencies. *Surface and Coatings Technology*, 263, 44-53. <https://doi.org/10.1016/j.surfcoat.2014.12.063>
- Farrag, A. A. G., & Balboul, M. R. (2017). Nano ZnO thin films synthesis by sol-gel spin coating method as a transparent layer for solar cell applications. *Journal of Sol-Gel Science and Technology*, 82, 269-279. <https://doi.org/10.1007/s10971-016-4277-8>
- Hacini, A., Ali, A. H., & Adnan, N. N. (2021). Optimization of ITO thin film properties as a function of deposition time using the swanepoel method. *Optical Materials*, 120, 111411. <https://doi.org/10.1016/j.optmat.2021.111411>

- Hu, J., & Gordon, R. G. (1992). Deposition of boron doped zinc oxide films and their electrical and optical properties. *Journal of The Electrochemical Society*, 139(7), 2014. <https://doi.org/10.1149/1.2221166>
- Jana, S., Vuk, A. S., Mallick, A., Orel, B., & Biswas, P. K. (2011). Effect of boron doping on optical properties of sol-gel based nanostructured zinc oxide films on glass. *Materials Research Bulletin*, 46(12), 2392-2397. <https://doi.org/10.1016/j.materresbull.2011.08.038>
- Kamaruddin, S. A., Chan, K. Y., Yow, H. K., Zainizan Sahdan, M., Saim, H., & Knipp, D. (2011). Zinc oxide films prepared by sol-gel spin coating technique. *Applied Physics A*, 104, 263-268. <https://doi.org/10.1007/s00339-010-6121-2>
- Kara, I., Atilgan, A., Serin, T., & Yildiz, A. (2017). Effects of Co and Cu dopants on the structural, optical, and electrical properties of ZnO nanocrystals. *Journal of Materials Science: Materials in Electronics*, 28, 6088-6092. <https://doi.org/10.1007/s10854-016-6285-4>
- Kaur, G., Mitra, A., & Yadav, K. L. (2015). Pulsed laser deposited Al-doped ZnO thin films for optical applications. *Progress in Natural Science: Materials International*, 25(1), 12-21. <https://doi.org/10.1016/j.pnsc.2015.01.012>
- Kayani, Z. N., Bashir, Z., Riaz, S., Naseem, S., & Saddiqe, Z. (2020). Transparent boron-doped zinc oxide films for antibacterial and magnetic applications. *Journal of Materials Science: Materials in Electronics*, 31, 11911-11926. <https://doi.org/10.1007/s10854-020-03745-5>
- Kim, S., Park, H., Nam, G., Yoon, H., & Leem, J. Y. (2013). Improved optical and electrical properties of sol-gel-derived boron-doped zinc oxide thin films. *Journal of sol-gel science and technology*, 67, 580-591. <https://doi.org/10.1007/s10971-013-3117-3>
- Kumar, V., Singh, R. G., Singh, F., & Purohit, L. P. (2012). Highly transparent and conducting boron doped zinc oxide films for window of Dye Sensitized Solar Cell applications. *Journal of alloys and compounds*, 544, 120-124. <https://doi.org/10.1016/j.jallcom.2012.07.124>
- Lee, S. H., Kim, M., Jung, Y., Jung, J. H., Kim, S., Leem, J. Y., & Kim, H. (2013). Enhanced optical and electrical properties of boron-doped zinc-oxide thin films prepared by using the sol-gel dip-coating method. *Journal of the Korean Physical Society*, 63, 1804-1808. <https://doi.org/10.3938/jkps.63.1804>
- Lokhande, B. J., Patil, P. S., & Uplane, M. D. (2001). Studies on structural, optical and electrical properties of boron doped zinc oxide films prepared by spray pyrolysis technique. *Physica B: Condensed Matter*, 302, 59-63. [https://doi.org/10.1016/S0921-4526\(01\)00405-7](https://doi.org/10.1016/S0921-4526(01)00405-7)
- Majerič, P., & Rudolf, R. (2020). Advances in ultrasonic spray pyrolysis processing of noble metal nanoparticles. *Materials*, 13(16), 3485. <https://doi.org/10.3390/ma13163485>
- Nečas, D., & Klapetek, P. (2012). Gwyddion: an open-source software for SPM data analysis. *Open Physics*, 10(1), 181-188. <https://doi.org/10.2478/s11534-011-0096-2>
- Ozel, K., & Atilgan, A. (2023a). Systematic Investigation on the Synergistic Impact of Gallium (Ga)-Boron (B) Co-Doping on the Features of ZnO Films. *Gazi University Journal of Science Part A: Engineering and Innovation*, 10(4), 442-451. <https://doi.org/10.54287/gujisa.1358177>
- Ozel, K., Atilgan, A., & Yildiz, A. (2023b). Multi-layered blocking layers for dye sensitized solar cells. *Journal of Photochemistry and Photobiology A: Chemistry*, 115297. <https://doi.org/10.1016/j.jphotochem.2023.115297>
- Ozel, K., & Yildiz, A. (2021). High-detectivity ultraviolet-B photodetector based on SnO₂ thin film/Si 30 heterojunction. *Semiconductor Science and Technology*, 36(9), 095001. <https://doi.org/10.1088/1361-6641/ac1051>
- Pawar, B. N., Jadkar, S. R., & Takwale, M. G. (2005). Deposition and characterization of transparent and conductive sprayed ZnO: B thin films. *Journal of Physics and Chemistry of Solids*, 66(10), 1779-1782. <https://doi.org/10.1016/j.jpcs.2005.08.086>

- Sbeta, M., Atilgan, A., Atli, A., & Yildiz, A. (2018). Influence of the spin acceleration time on the properties of ZnO: Ga thin films deposited by sol-gel method. *Journal of Sol-Gel Science and Technology*, 86, 513-520. <https://doi.org/10.1007/s10971-018-4652-8>
- Senol, S. D., Ozturk, O., & Terzioğlu, C. (2015). Effect of boron doping on the structural, optical and electrical properties of ZnO nanoparticles produced by the hydrothermal method. *Ceramics International*, 41(9), 11194-11201. <https://doi.org/10.1016/j.ceramint.2015.05.069>
- Smirnov, M., Baban, C., & Rusu, G. I. (2010). Structural and optical characteristics of spin-coated ZnO thin films. *Applied Surface Science*, 256(8), 2405-2408. <https://doi.org/10.1016/j.apsusc.2009.10.075>
- Steinhauser, J., Fay, S., Oliveira, N., Vallat-Sauvain, E., & Ballif, C. (2007). Transition between grain boundary and intragrain scattering transport mechanisms in boron-doped zinc oxide thin films. *Applied Physics Letters*, 90(14). <https://doi.org/10.1063/1.2719158>
- Sun, Y. T. A., Pan, P. C., Koo, H. S., & Lin, N. Y. (2020). Growth of low resistivity and high transparency boron-doped zinc oxide film by pulse laser deposition. *Precision Engineering*, 66, 605-610. <https://doi.org/10.1016/j.precisioneng.2020.08.001>
- Tahar, R. B. H., & Tahar, N. B. H. (2005). Boron-doped zinc oxide thin films prepared by sol-gel technique. *Journal of materials science*, 40, 5285-5289. doi:10.1007/s10853-005-0522-1
- Tan, S. T., Chen, B. J., Sun, X. W., Fan, W. J., Kwok, H. S., Zhang, X. H., & Chua, S. J. (2005). Blueshift of optical band gap in ZnO thin films grown by metal-organic chemical-vapor deposition. *Journal of Applied Physics*, 98(1). <https://doi.org/10.1063/1.1940137>
- Zhussupbekova, A., Caffrey, D., Zhussupbekov, K., Smith, C. M., Shvets, I. V., & Fleischer, K. (2020). Low-cost, high-performance spray pyrolysis-grown amorphous zinc tin oxide: the challenge of a complex growth process. *ACS Applied Materials & Interfaces*, 12(41), 46892-46899. 3. <https://doi.org/10.1021/acsami.0c12148>